Science Advances
AAAS

advances.sciencemag.org/cgi/content/full/6/44/eaba7702/DC1

Supplementary Materials for

Harnessing lipid signaling pathways to target specialized pro-angiogenic neutrophil subsets for regenerative immunotherapy

T. C. Turner, M. C. P. Sok, L. A. Hymel, F. S. Pittman, W. Y. York, Q. D. Mac, S. Vyshnya, H. S. Lim, G. A. Kwong, P. Qiu, E. A. Botchwey*

*Corresponding author. Email: edward.botchwey@bme.gatech.edu

Published 30 October 2020, *Sci. Adv.* **6**, eaba7702 (2020)
DOI: 10.1126/sciadv.aba7702

This PDF file includes:

Figs. S1 to S10

Supplementary Materials

Fig. S1.

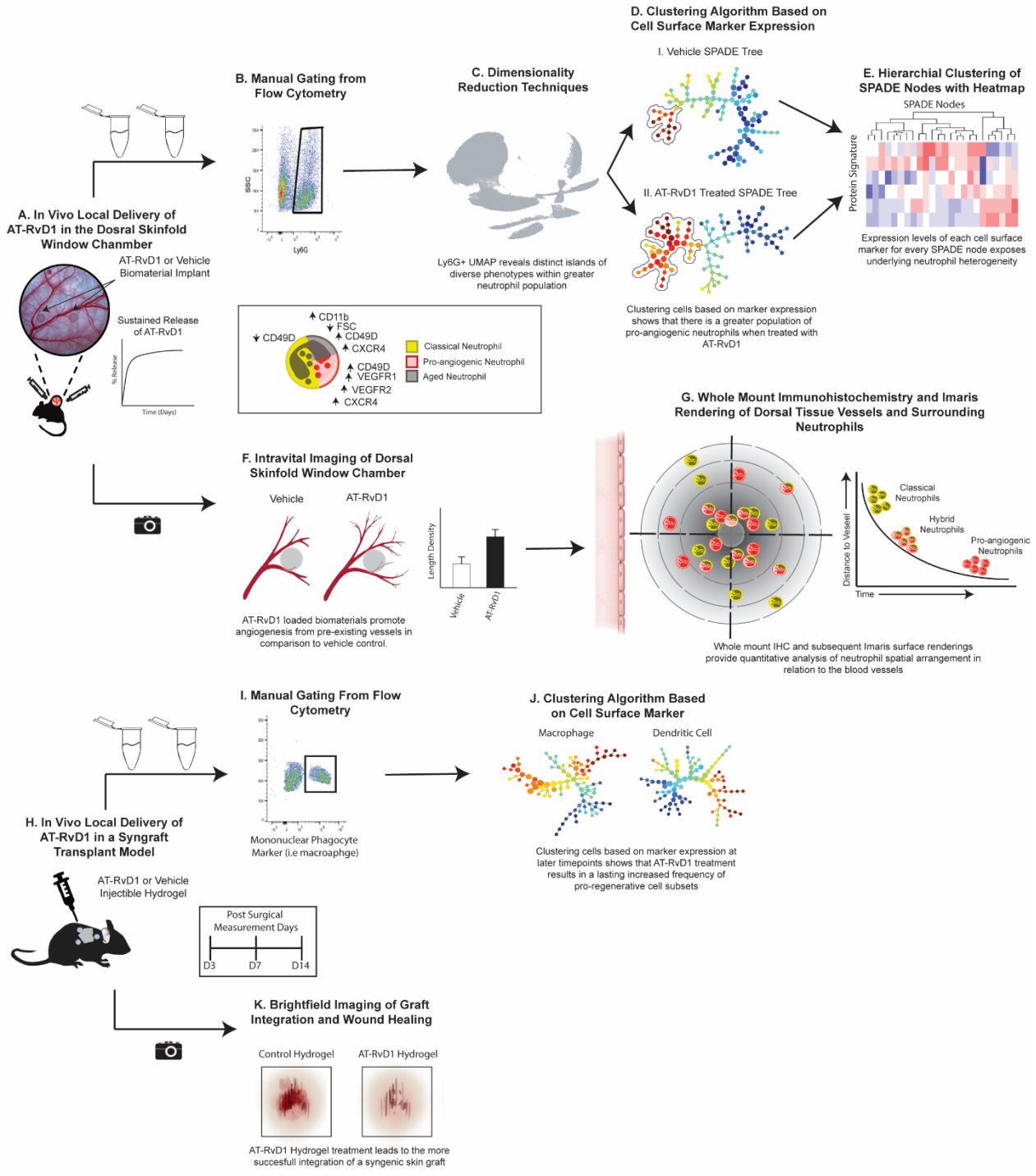

Fig. S1. A model workflow for characterizing neutrophil inflammation heterogeneity. Our approach utilizes high dimensional single-cell flow cytometry data and complementary dimensionality reduction algorithms to generate a 2D projection of immune cell heterogeneity **(A to E)**. Subsequent steps infer a functional role for immune cell subsets based on spatial distribution of infiltrating cells within damaged tissues as well as responsiveness to AT-RvD1 treatment **(A, F, and G)**. This approach is used in a different model and with a different delivery platform **(H-K)** to validate the therapeutic potential of AT-RvD1 delivery.

Fig. S2.

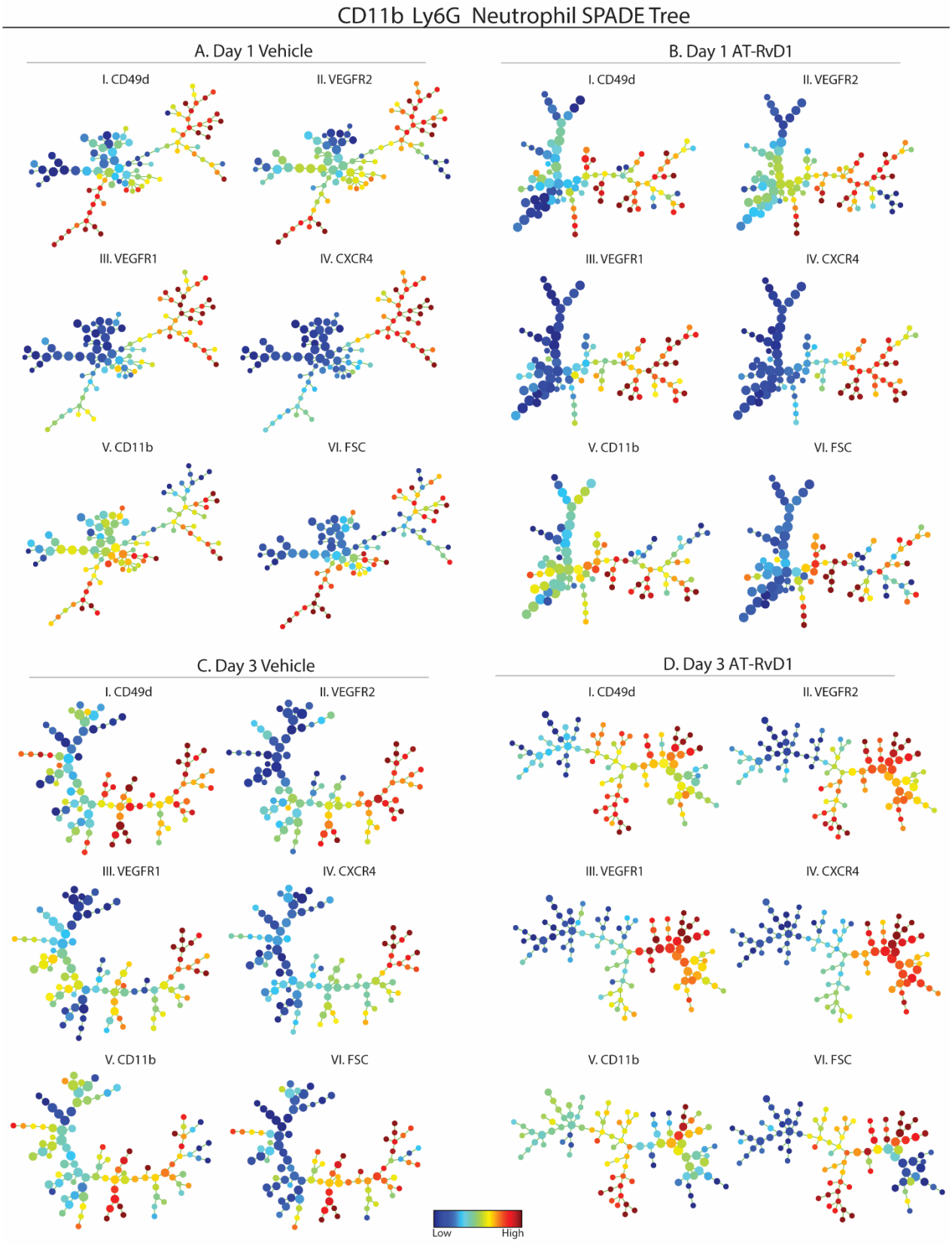

Fig. S2. SPADE marker expression array informs neutrophil subset identification. Pseudotime analysis generated SPADE trees consisting of CD11b+Ly6G+ neutrophils from tissue at day 1 after surgery with vehicle control **(A)**, day 1 after surgery with sustained AT-RvD1 treatment **(B)**, day 3 after surgery with a vehicle control **(C)**, and day

3 after surgery with sustained AT-RvD1 treatment **(D)**. An array of six trees that have a marker expression heatmap overlay is generated for each condition **(I-VI)**. The marker expressions shown are CD49d **(I)**, VEGFR2 **(II)**, VEGFR1 **(III)**, CXCR4 **(IV)**, CD11b **(V)** and FSC **(VI)** with blue colors indicating a node with low expression and red colors indicating a node with high expression of the respective marker.

Fig. S3.

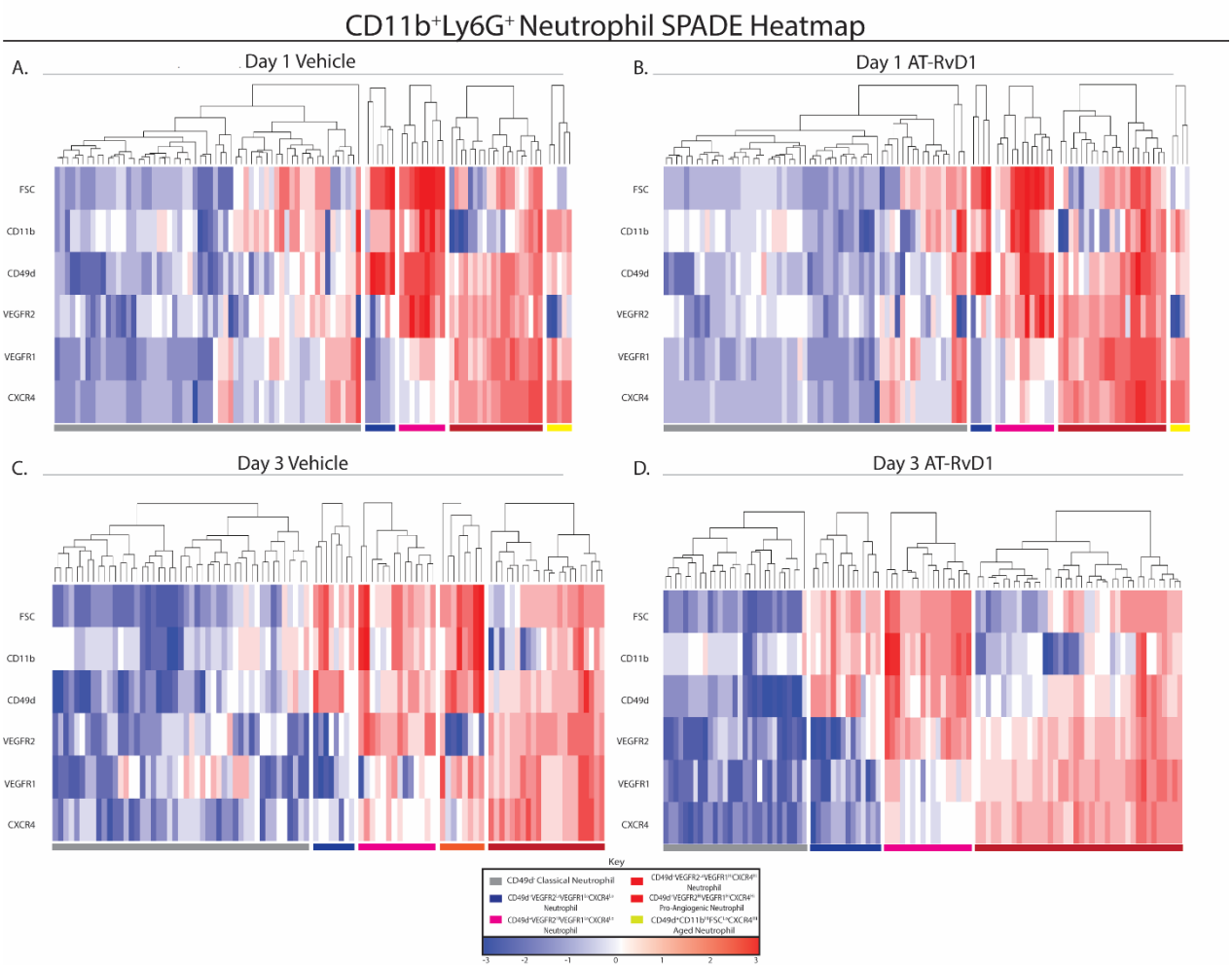

Fig. S3. Marker expression heatmap of SPADE nodes reveals subtle neutrophil heterogeneity. Every node of the SPADE tree has a distinct surface marker fingerprint that can be shown using a heatmap. Heatmap showing marker expression (rows) in every node (column) of the day 1 vehicle control **(A)**, day 1 AT-RvD1 treated **(B)**, day 3 vehicle control **(C)** and day 3 AT-RvD1 treated **(D)** $Ly6G^+$ SPADE dendrograms shown in Fig.3. The colors along the bottom of each heatmap correspond to the neutrophil phenotypes identified using the corresponding SPADE tree. The marker expression shown is reported using a z-score calculated using the mean and standard deviation of every marker expression where the population is $CD11b^+Ly6G^+$ Neutrophils. Blue shows an expression level below the mean of the population and red shows an expression level above the mean of the population.

Fig. S4.

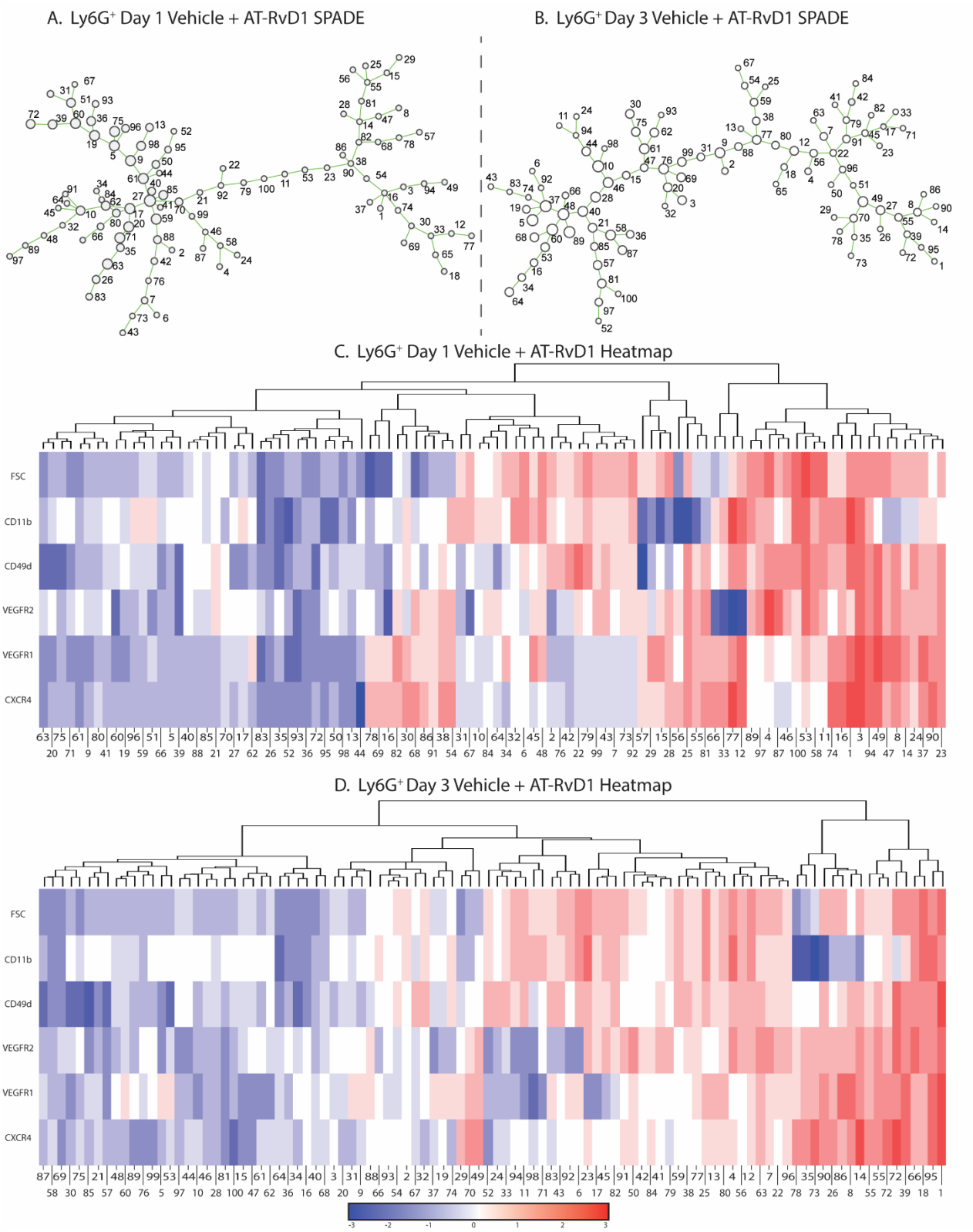

Fig. S4. Combined day 1 and day 3 SPADE dendrogram for tornado plot analysis. SPADE dendrogram from pre-gated CD11b^{+}Ly6G^{+} neutrophils from day 1 **(A)** and day 3 **(B)** tissue of pooled vehicle and AT-RvD1 treated samples with numbered nodes. Heatmap showing marker expression (rows) in every node (column) of the day 1 **(C)** and day 3 **(D)** Ly6G+ SPADE dendrograms **(A and B)**.

Fig. S5.

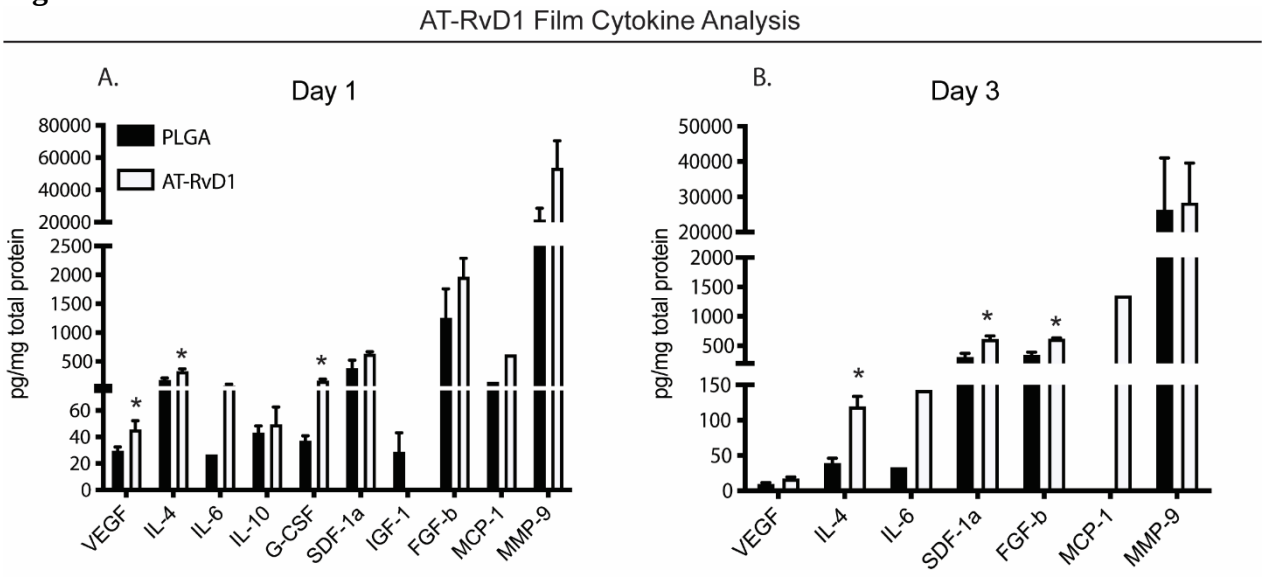

Fig S5. Local Delivery of AT-RvD1 modulates the cytokine profile. Expression levels of the cytokines included in the multiplex cytokine analysis at day 1 **(A)** and day 3 **(B)**. Data presented as mean ± S.E.M. Statistical analysis were preformed using two-way ANOVA with Tukey's post-hoc test *$p < 0.05$. n = 1-3 animals per group.

Fig. S6.

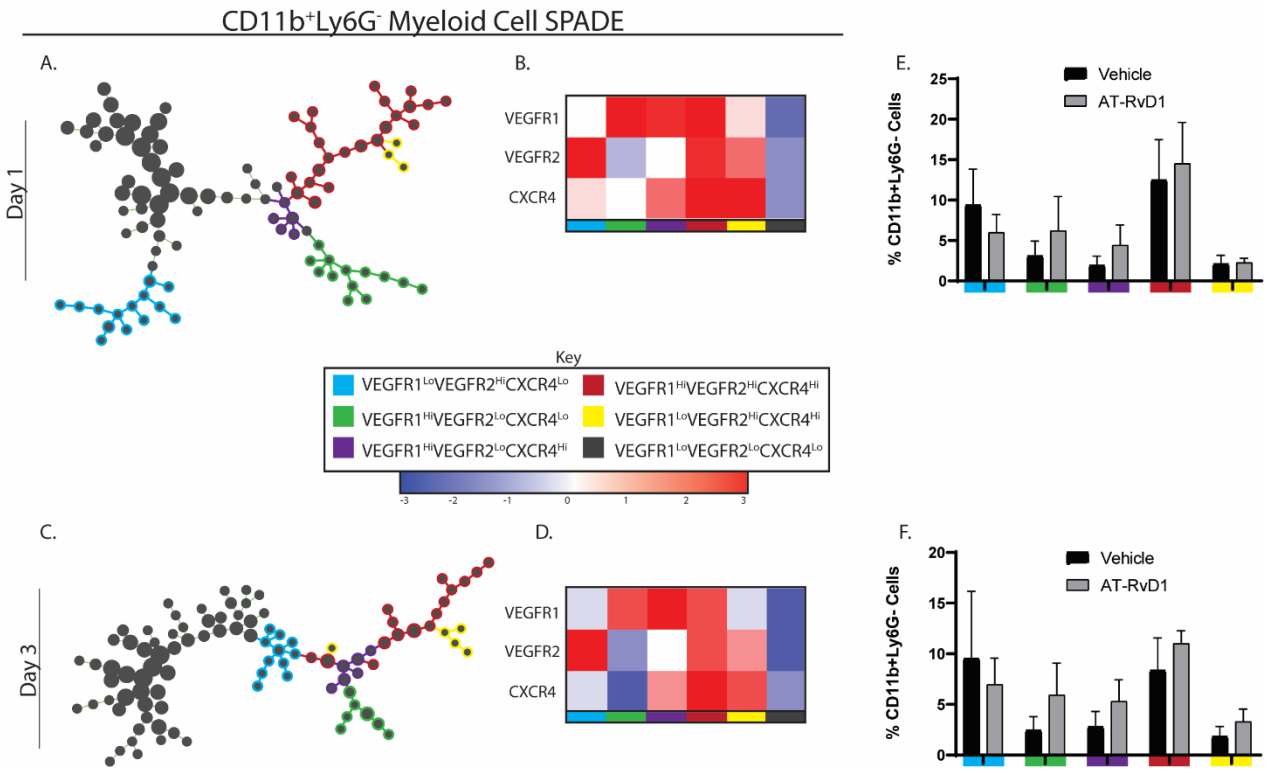

Fig S6. AT-RvD1 treatment does not modulate CD11b+Ly6G- myeloid cells expressing pro-angiogenic surface markers. SPADE dendrograms were constructed using CD11b+Ly6G- cells at day 1 **(A)** and day 3 **(C).** Both dendrograms were annotated using combinations of high and low VEGFR1, VEGFR2, and CXCR4 expression **(B and D)**. These groups were then quantified

and show no significant differences with AT-RvD1 treatment at both timepoints **(E and F)**. Statistical analyses were performed using a two-way anova with Tukey's multiple comparisons, *p < 0.05, ** p < 0.01, *** p < 0.001, **** p < 0.0001, n = 4 animals per group.

Fig. S7.

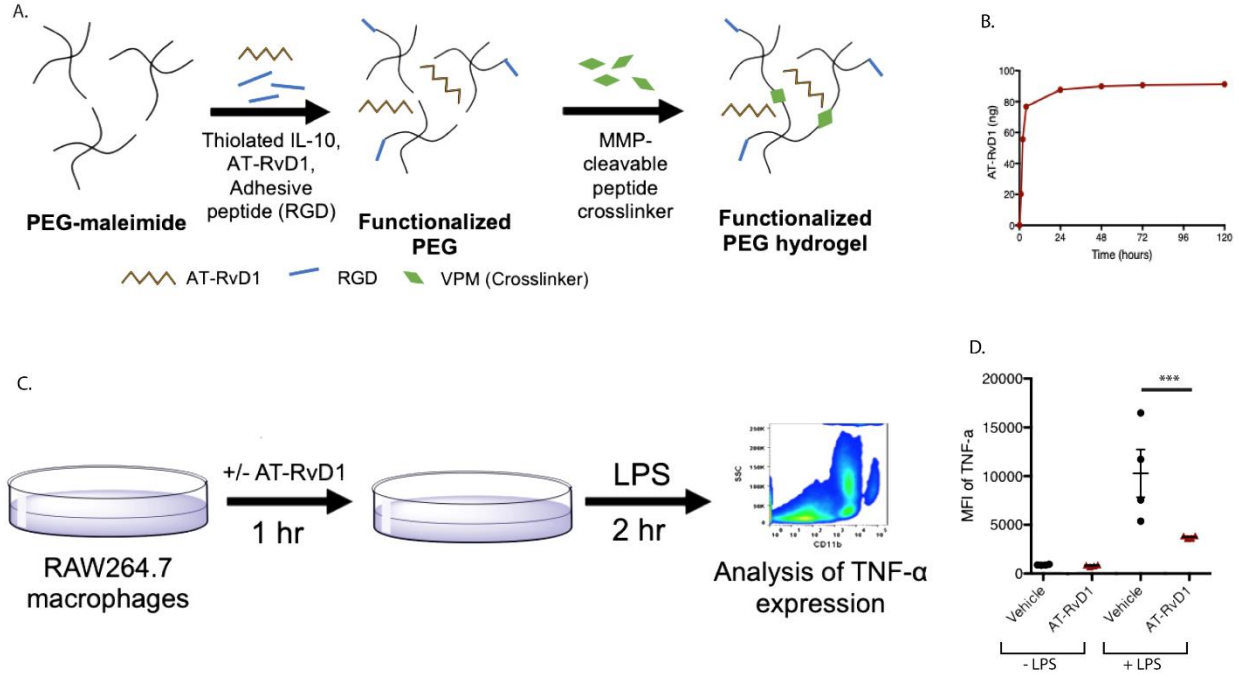

Fig S7. Hydrogel schematics, release profiles, and bioactivity. Hydrogel fabrication method **(A)** HPLC measurements of AT-RvD1 release from PEG-MAL hydrogels **(B)**. Bioactivity assay schematic **(C).** Bioactivity of AT-RvD1 **(D)**. Statistical analysis was performed using one-way ANOVA with Tukey's post-hoc test, ***p<0.001, n=4.

Fig. S8.

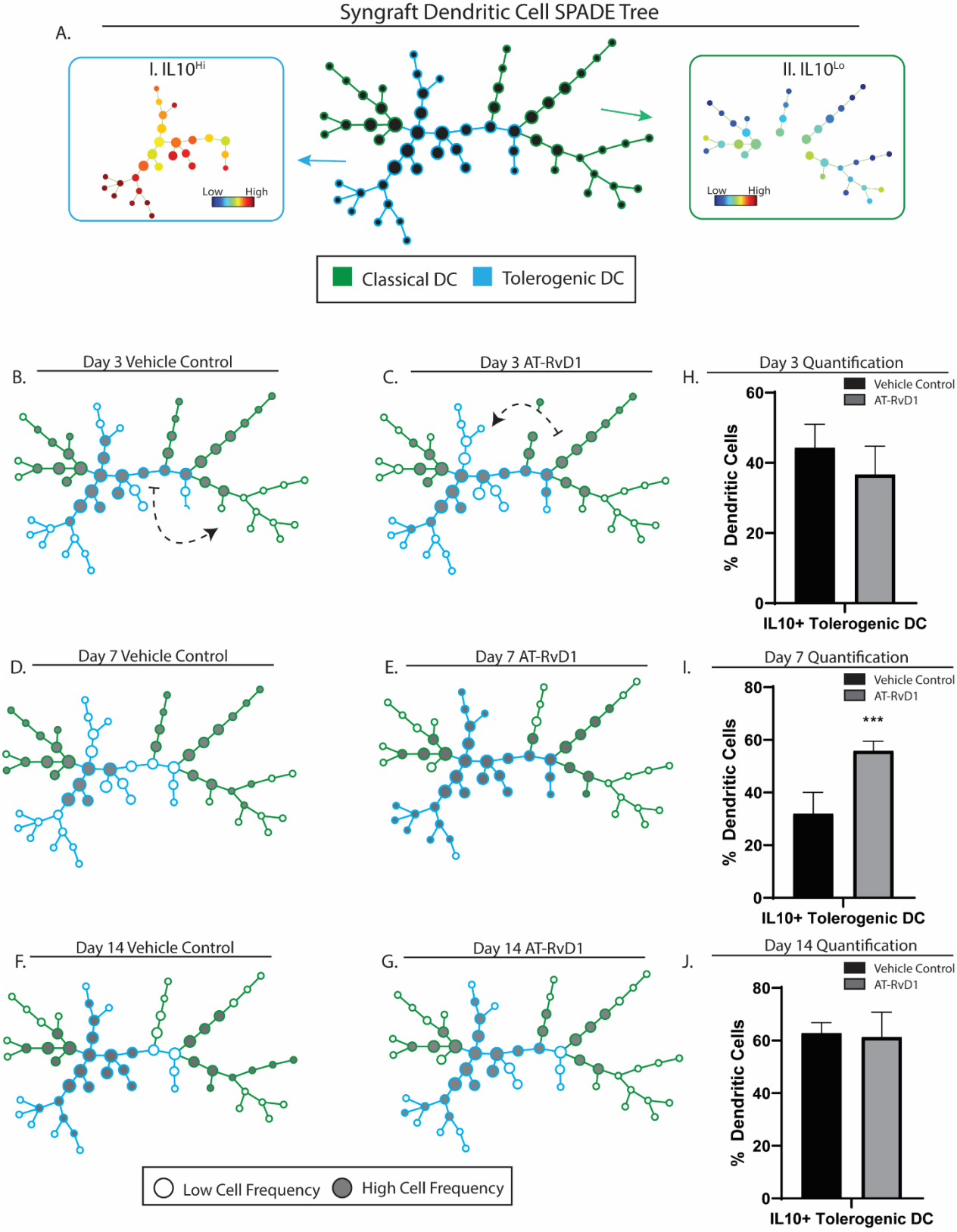

Fig. S8. AT-RvD1 promotes a pro-regenerative shift of the dendritic cell population. CD11c+ dendritic cells pooled from all samples from both treatments and three timepoints (day 3, 7, and 14) were used to construct a SPADE dendrogram **(A)**. This SPADE dendrogram is annotated according to il10 surface marker expression. The blue annotation corresponds to a

tolerogenic phenotype with high Il10 expression **(I)** and the green annotation corresponds to a classical phenotype with low il10 expression **(II)**. Cells corresponding to a specific timepoint and treatment combination are isolated and mapped out on the SPADE dendrogram to analyze where these cells are highly populated (grey nodes) and where they are less densely populated (white nodes) **(B-G)**. The movement of these cells across time is depicted with dashed arrows that show where the cells are visualized to move **(B and C)**. The visualization method shows an AT-RvD1 mediated shift in cell frequency towards a tolerogenic phenotype that can also be seen in the corresponding quantifications **(H-J)**. Data presented as mean ± S.E.M. Statistical analyses were performed using two-tailed t-tests ***p < 0.001 n = 4 animals per group.

Fig. S9.

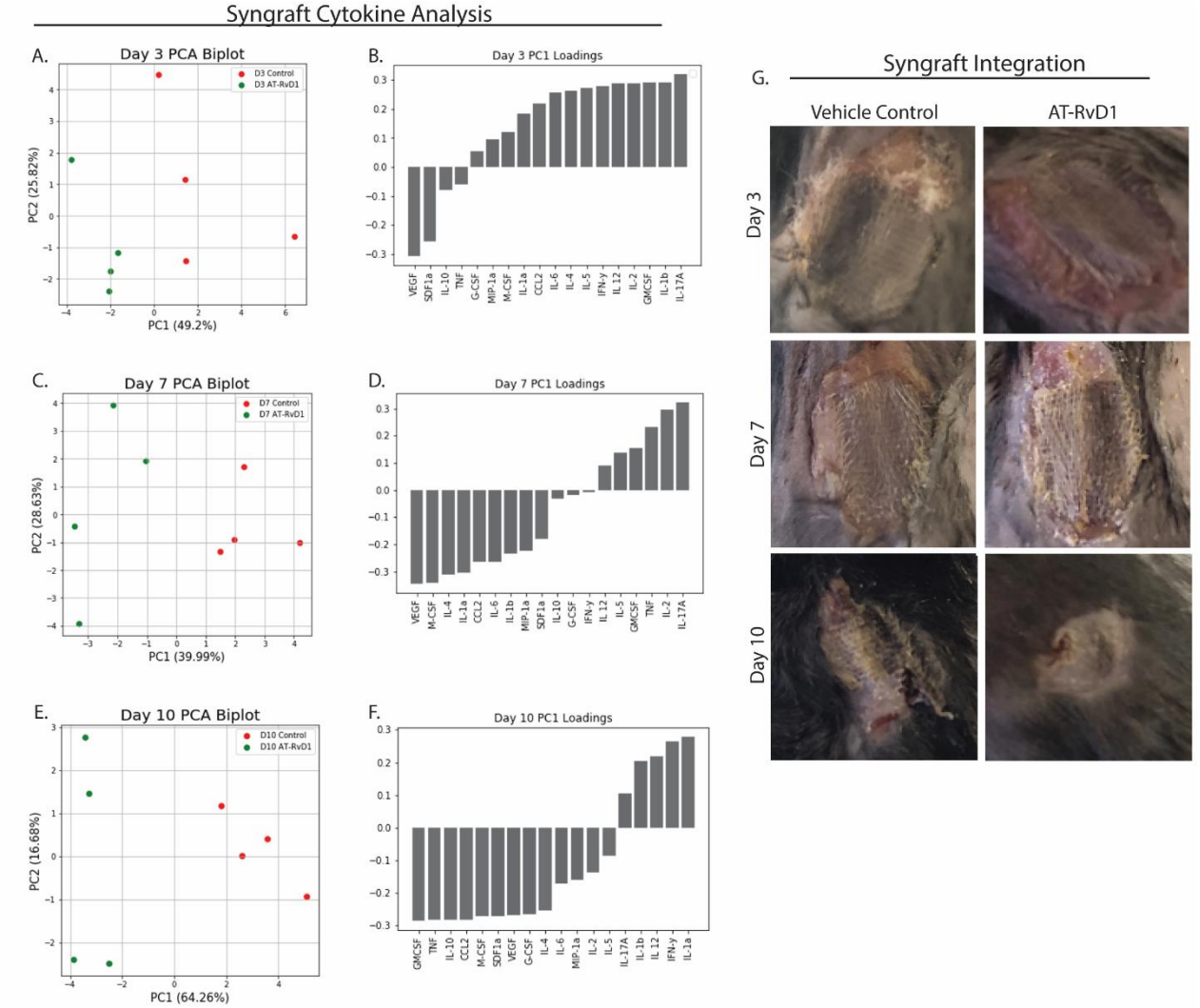

Figure S9. Multiplex cytokine analysis and macroscopic image analysis of AT-RvD1 treatment compared to vehicle control. Principal components analysis was performed at days 3, 7 and 10 on a multiplex cytokine panel **(A-F)**. At all three timepoints AT-RvD1 treated samples are shown to separate along component 1 **(A, C and E)**. The loadings plots shows the cytokines that contribute the most to this separation **(B, D and F)**. Macroscopic images of graft integration show increased wound closure with AT-RvD1 treatment. Photo Credit: M.C.P Sok, Wallace H. Coulter Department of Biomedical Engineering, Georgia Institute of Technology and Emory University **(G)**.

Fig. S10.

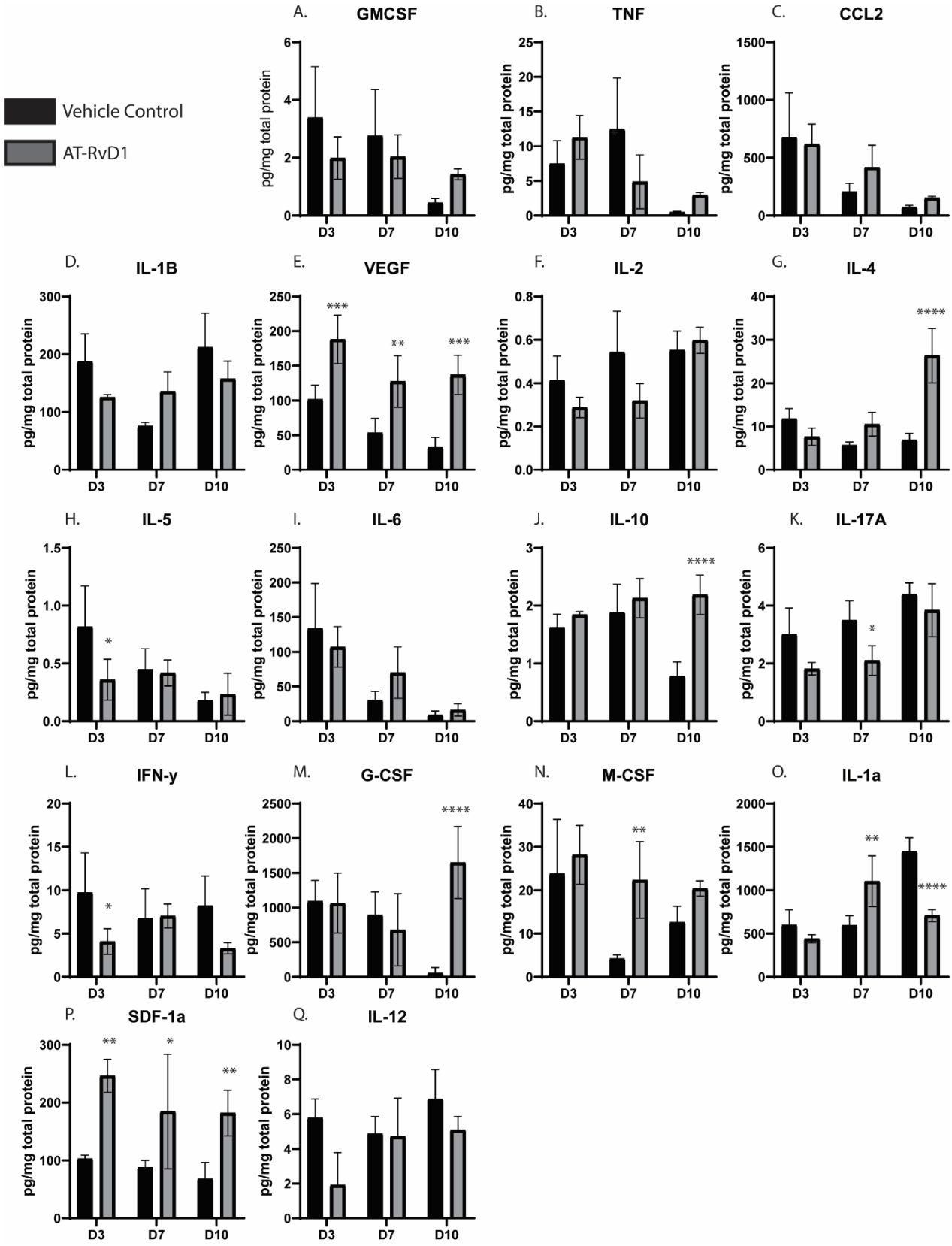
Vehicle Control
AT-RvD1
A. GMCSF
B. TNF
C. CCL2
D. IL-1B
E. VEGF
F. IL-2
G. IL-4
H. IL-5
I. IL-6
J. IL-10
K. IL-17A
L. IFN-y
M. G-CSF
N. M-CSF
O. IL-1a
P. SDF-1a
Q. IL-12
pg/mg total protein
D3
D7
D10

Figure S10. At-RvD1 increases concentration of anti-inflammatory cytokines in the peri-implant environment. A comparison of various cytokine levels between AT-RvD1 treatment and vehicle control at days 3, 7 and 10 **(A-Q)**. Data presented as mean ± S.E.M. Statistical analysis were preformed using two-way ANOVA with Tukey's post-hoc test *$p < 0.05$. n = 4 animals per group.